AKARI sheds light on the red side of active galactic nuclei at $z = 0$ to $z = 6$

Myungshin Im[1]

[1] *CEOU, Astronomy program, Department of Physics & Astronomy, Seoul National University, 1 Gwanak-rho, Gwanak-gu, Seoul, 08826, Republic of Korea*

ABSTRACT

This paper presents highlights from *AKARI* studies of active galactic nuclei (AGNs). Using its unique spectroscopic capability at 2.5 to 5.0 μm, *AKARI* revealed for the first time the redshifted Hα lines and the rest-frame optical spectra of AGNs at $4 < z < 6$, establishing the luminosity scaling relations in the optical at high redshift and tracing the black hole mass growth history in the early universe based on black hole (BH) mass estimators in the optical. The *AKARI*'s NIR spectroscopy also helped researchers detect the Brackett lines and 3.3 μm PAH features and traced the hot/warm dust emission of nearby AGNs and luminous infrared galaxies, showing promises of these spectral features to examine the host galaxy star formation rate and the black hole masses. The NIR spectroscopy of low redshift AGNs also revealed a rather cooler nature of the hot dust emission with $T \sim 1100$ K than previously discussed. *AKARI* also produced other interesting scientific results utilizing its pan-chromatic mid-infrared (MIR) imaging capability. *AKARI* made pioneering contributions to the MIR selection of obscured/unobscured AGNs, two-sided nature of AGN feedback in the galaxy evolution, and the AGN contribution in luminous infrared galaxies. These results pave ways for infrared studies of AGN by post-*AKARI*/future facilities and we expect that studies of the data gained by *AKARI* will continue to make valuable contributions to our understanding of AGNs.

Keywords: Active galactic nuclei, Quasars, Galaxy evolution, High redshift universe

1. INTRODUCTION

Galaxies often harbor active central regions that are powered by supermassive black holes (SMBHs). These active nuclear regions are called Active Galactic Nuclei (AGNs). AGNs emit energetic photons in X-ray and ultra-violet (UV) from their accretion disks, as well as cold photons in far-infrared (FIR) from star forming regions surrounding SMBHs (Figure 1). Since AGN spectral energy distribution (SED) spans over this wide wavelength range, it is necessary to perform a mutli-wavelength study to gain a full understanding on the physical processes that occur in AGNs. In particular, infrared (IR) observation is crucial to understand the following areas of AGN physics.

Fisrt, IR study of AGNs can give us information on the dust torus and star formation activities in AGN. The unification picture of AGN (Urry & Padovani 1995) describes that SMBHs in AGNs have accretion disks that are surrounded by broad line region clouds (BLRs). The BLRs are responsible for broad emission lines. Beyond BLRs, there is a dust torus that obscures the light from the central engine and BLRs. In NIR, the emission from the hot dust torus outshines the host galaxy light, and studying the NIR continuum can give us insights on the dust torus. Similarly in mid-infrared (MIR), warm dust emission dominates the light, which arises from a different part of the dust torus. In FIR, one finds the reprocessed UV light from star formation activities of AGN host galaxies, and hence it is imperative to study FIR to understand the co-evolution of supermassive black holes (SMBHs) and their host galaxies.

Second, NIR is a window where useful AGN diagnostic emission lines are redshifted. For example, hydrogen Balmer lines are commonly used to measure BH masses (e.g., Vestergaard & Peterson 2006), but at $z > 3.5$, the most prominent Balmer line, Hα, is redshifted to $\lambda > 2.5$ μm where the bright thermal background prohibits faint object spectroscopy from the ground. Since hydrogen Balmer lines are used as a primary BH mass estimator from which secondary estimators using UV lines such as Mg II or C IV are derived, performing NIR spectroscopy at 2.5 μm $< \lambda <$ 5.0 μm is valuable to test the reliability of UV-based BH mass estimators at high redshift. On the other, hydrogen Paschen or Brackett lines of low to moderate redshift AGNs offer unique opportunities to estimate AGN BH masses where the dust extinction is much smaller in comparison to the Balmer lines (e.g., Kim et al. 2010). Similarly to the high redshift Balmer lines, these lines require sensitive NIR spectroscopy at $\lambda > 2.5$ μm. The PAH 3.3 μm feature is another interesting NIR spectral feature

Corresponding author: Myungshin Im
mim@astro.snu.ac.kr

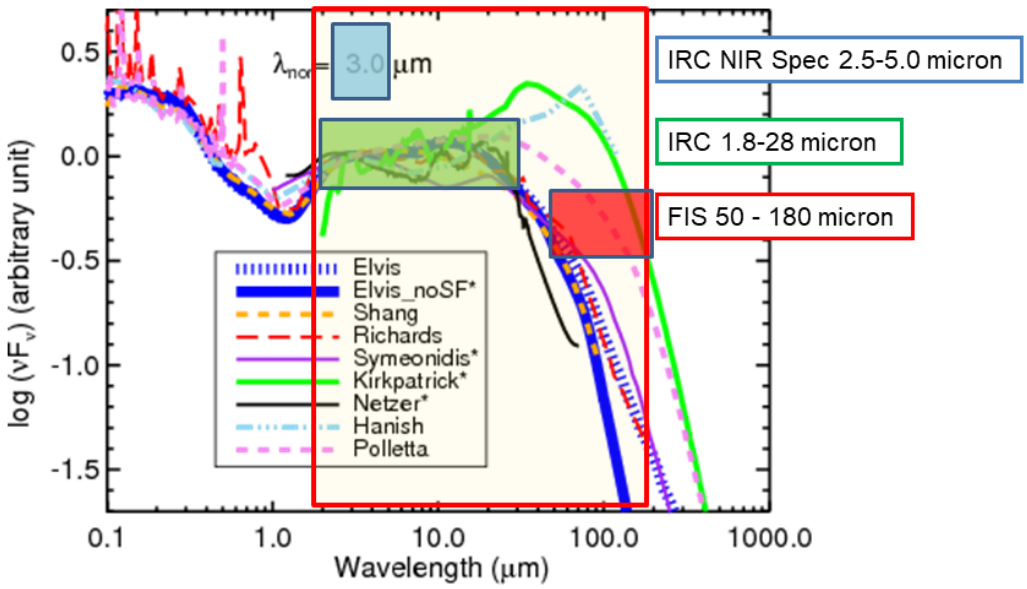

Figure 1. Spectral energy distributions of AGNs from UV to FIR. We also indicate which parts of the AGN SEDs are covered by *AKARI*. *AKARI* can study the hot/warm dust emission at NIR and MIR, as well as FIR emission. *AKARI* also obtained NIR/MIR spectra at 2.5 to 5.0 μm and in MIR. The background figure of the AGN SED is taken from Lyu & Rieke (2017).

that can be used to study star formation rate (SFR) of dusty galaxies (Kim et al. 2012; Yamada et al. 2013), and can be observed with future sensitive space telescopes (e.g., the *James Webb Space Telescope; JWST*) even at high redshift.

Armed with near-infrared spectroscopic capability of $R \sim 100$ at 2.0 μm $< \lambda <$ 5.0 μm, and the imaging capability that covered the wavelength regions from 1.8 to 28 μm (Infrared Camera (IRC); Onaka et al. 2007) and also from 50 to 180 μm (Far-Infrared Surveyor (FIS); Kawada et al. 2007), *AKARI* (Murakami et al. 2007) performed unique investigation of the red side of AGNs. Here, we review some of the highlights of *AKARI* AGN studies. Many interesting AGN studies have been made with *AKARI*, and we regret that we only present a rather partial view unintentionally. Interested readers are strongly advised to check other contributions in this proceedings where some of the interesting AGN studies not covered by this article are presented.

2. MIR SELECTION OF AGN

AKARI IRC performed imaging at 2, 3, 4, 7, 9, 11, 15, 18, and 24 μm, among which 11 μm and 15 μm imaging capabilities were unique in comparison to *Spitzer*. AGNs are known to have a rising NIR and MIR SED which is different from the SEDs of galaxies and stars. Hence, AGNs generally have NIR and MIR colors that are almost always red. Also, NIR and MIR wavelengths are where the effect of dust extinction is relatively mild, making the NIR/MIR-based selection of AGNs less sensitive to the dust extinction than the UV/optical color-based methods. In this regard, *AKARI* made a pioneering contribution to the MIR color selection of AGNs.

Figure 2 shows a *AKARI* MIR-color selection of AGNs in the *AKARI* North Ecliptic Pole (NEP) survey field (Matsuhara et al. 2006; Lee et al. 2009). Here, $N2$ (2 μm) $-$ $N3$ (3 μm) versus $S7$ (7 μm) $-$ $S11$ (11 μm) color-color diagram selects AGNs effectively (Lee et al. 2007). In Figure 2, we also plot spectroscopically identified objects as crosses (Shim et al. 2013), among which AGNs are marked with circles and star forming galaxies are the rest. Spectroscopically identified type 1 AGNs (blue circles) are clustered in the region where both $N2 - N3$ and $S7 - S11$ colors are greater than 0 as expected, and they are well separated from the spectroscopically identified star-forming (SF) galaxies This is the first time that 11 μm data is utilized in conjunction with the other MIR photometry points for AGN selection, well before the *WISE* color selection of AGNs were put forward (e.g., Jarrett et al. 2011; Mateos et al. 2012; Hwang & Geller 2013). A similar *AKARI* MIR-based AGN selection is presented in Hanami et al. (2012).

A significant number of AGNs are expected to be dusty, and therefore uncovering the obscured AGN population is important to gain a complete view of the AGN population. Dusty, obscured AGNs can be found effectively, when combining *AKARI* IR data with other wavelength data. In particular, obscured AGNs can be selected with X-ray satellites such as *MAXI* and *Chandra*, and a number of diagnostics have been proposed to identify Compton-thick AGNs this way (Isobe et al. 2016; Krumpe et al. 2015). Isobe et al. (2016) used the hardness ratio and the ratio of the X-ray emission over 18 μm flux to separate Compton-thick AGNs from other types of AGNs. Seyfert 2 AGNs, in general, have low L_S/L_{18} ratios (L_S: soft X-ray flux; L_{18}: 18 μm flux) in comparison to Seyfert 1 AGNs. If they are Compton-thick, their hardness ratios decrease considerably. This way, they were able to identify NGC 1365 as a Compton-thick AGN with the absorption column density as high as $N_{\rm H} \sim 4 \times 10^{24}$ cm^{-2}. This kind of study can be extended to higher redshift AGNs. Krumpe et al. (2015) studied IR sources in the *AKARI* NEP field, and used the characteristic MIR SED of AGNs to isolate

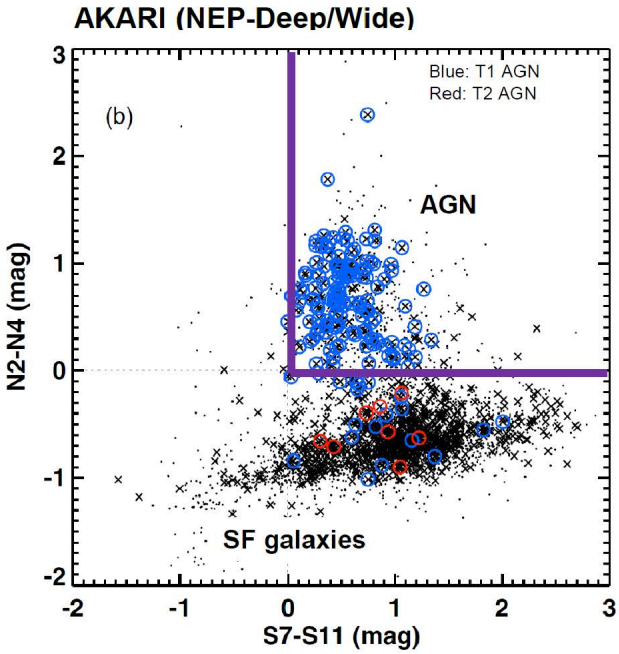

Figure 2. The AGN selection method that is based on the *AKARI* MIR colors. AGNs are selected as objects having $S7 - S11 > 0$ and $N2 - N4 > 0$, while star forming galaxies are those outside the box. Blue circles denote the spectroscopically confirmed type 1 AGNs and the red circles indicate the spectroscopically confirmed type 2 AGNs. The remaining crosses indicate spectroscopically identified star forming galaxies. Also see Lee et al. (2007).

IR-selected AGNs (following Hanami et al. 2012 prescription), and they further selected the Compton-thick IR-selected AGNs as those having low $L_{\rm obs,2-7kev}/L_{\rm IR,AGN}$ ratios. This way, Krumpe et al. (2015) selected 26 Compton-thick AGNs in the *AKARI* NEP field.

3. PAH3.3, HYDROGEN BRACKETT LINES, AND OBSCURATION OF AGN

Ultra-luminous infrared galaxies (ULIRGs) are heavily dust-enshrouded star forming galaxies that are also thought to harbor obscured AGNs. The *AKARI* 2.5–5.0 μm spectroscopy offered a way to investigate if there is a hidden AGN in such a system. In a system where the dust -heating source is dominated by starburst activities, the star forming regions are expected to be uniformly distributed and in such a case, one would see the PAH 3.3 μm feature (hereafter, PAH3.3) to be visible in emission. On the other hand, the systems dominated with hidden AGNs at center would have PAH3.3 absorption features in the rising NIR-MIR SED. Imanishi et al. (2010a,b) examined the PAH3.3 feature in IR luminous galaxies, finding that the fraction of buried AGNs increases as $L_{\rm IR}$ increases, suggesting the growth of SMBHs at centers of ULIRGs.

The PAH3.3 feature has been suggested as a useful star formation indicator too (Kim et al. 2012; Yamada et al. 2013). Type 1 AGNs show PAH emission features and this has been used to infer the star formation rate in AGN (Kim, J. H. et al., in preparation). Kim et al. (2017, in preparation) studied the PAH3.3 emission in 49 PG quasars, and the preliminary results show that the luminosity of PAH3.3 (SF indicator) correlates with the 5100 Å luminosity (AGN activity indicator), suggesting a strong tie between AGN and SF.

The *AKARI* NIR spectroscopic data provide useful diagnostics to study red, obscured AGNs. *AKARI* performed a 2.5–5.0 μm spectroscopic study of low redshift AGNs as a part of the program, Quasar Spectroscopic Observation with NIR Grism (QSONG) where NIR spectra of 83 nearby AGNs and red AGNs were obtained (Im 2010, 2017; Kim et al. 2015). QSONG also targeted 155 high redshift quasars, and we will discuss the results from the high redshift quasars in Section 6. Using the QSONG data, Kim et al. (2015) studied NIR spectra of low redshift type 1 AGNs and detected the hydrogen Brackett lines and PAH3.3 lines in some of them. The *AKARI* spectrum of NGC 4151 is shown as an example to show the rich spectroscopic information in the NIR wavelength region (Figure 3). By fitting the broad Brackett lines, they showed that Brackett line luminosities and line widths correlate well with those of the Balmer lines. Then they derived the BH mass estimator using the Brackett line luminosities and widths as shown in Figure 4 and Equations (1) and (2). Since NIR hydrogen lines such as the Brackett lines are much less extincted than the Balmer lines by dust, it is important to establish BH mass estimators using NIR hydrogen lines for studying red, dusty AGNs. For example, at $E(B-V) = 2.0$ which is a typical color excess value of red quasars (e.g, Urrutia et al. 2009), the Hβ line gets suppressed by a factor of

1000, but the Brα or Brβ line fluxes get suppressed only by factors of 1.3 and 1.6 respectively. From the QSONG data, Kim et al. (2015) derive the Brackett line $M_{\rm BH}$ estimators as,

$$\log(M_{\rm BH}/M_\odot) = 6.61 \pm 0.23 + (0.68 \pm 0.13) \times \log(\frac{L_{{\rm Br}\beta}}{10^{40}{\rm erg\,s^{-1}}}) + 2\log(\frac{\sigma_{{\rm Br}\beta}}{10^3{\rm km\,s^{-1}}}), \quad (1)$$

and

$$\log(M_{\rm BH}/M_\odot) = 6.68 \pm 0.20 + (0.66 \pm 0.21) \times \log(\frac{L_{{\rm Br}\alpha}}{10^{40}{\rm erg\,s^{-1}}}) + 2\log(\frac{\sigma_{{\rm Br}\beta}}{10^3{\rm km\,s^{-1}}}). \quad (2)$$

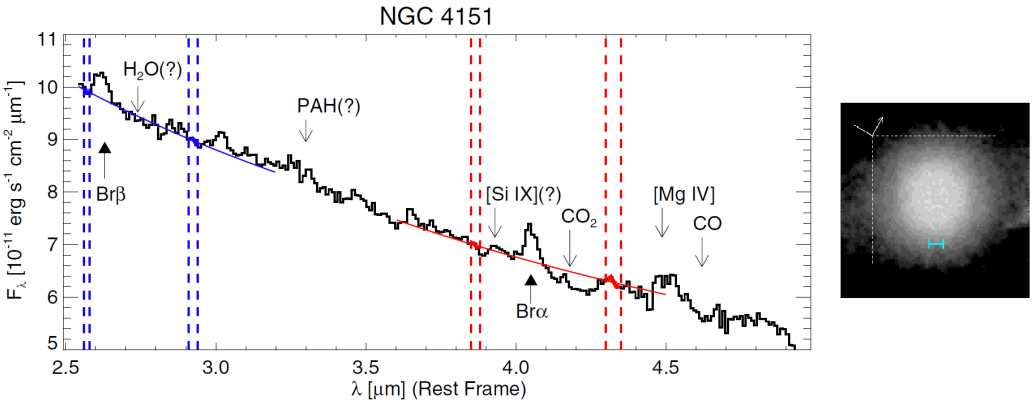

Figure 3. The *AKARI* 2.5–5.0 μm spectrum of NGC 4151. Several NIR hydrogen lines and molecular lines are indicated, showing the rich information contained in the *AKARI* data. The postage stamp image on the right shows the image from the digitized sky survey (DSS), where the white dashed line indicates the 1′ by 1′ aperture window over which the spectrum was taken and the horizontal cyan bar shows a 7.″3 extraction window which was used for constructing the 1-dimensional spectrum on the left. Reproduced from Figures in Kim et al. (2015).

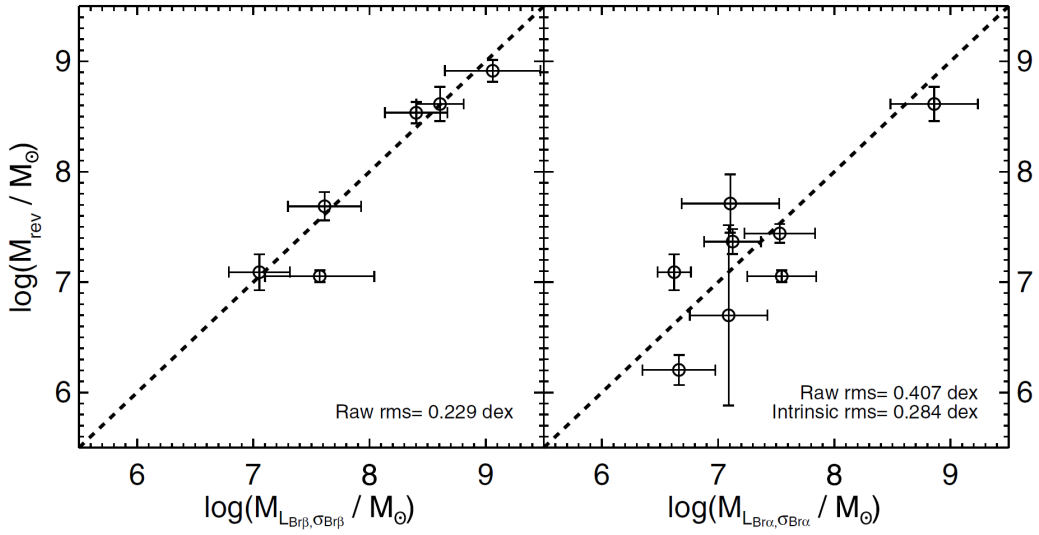

Figure 4. Comparison of $M_{\rm BH}$ values from the reverberation mapping method versus the Brackett line estimators. The rms scatters in this correlations are 0.2 and 0.4 dex respectively. The intrinsic scatter is not measurable for the Brβ case, while it is 0.28 dex for the Brα. The reasonable agreement between the two quantities suggests that the Brackett lines can be used to estimate $M_{\rm BH}$. This picture is taken from Kim et al. (2015).

In a different work, both the Brα line and the PAH3.3 feature were used to investigate the contribution of AGN in ULIRG. Yano et al. (2016) investigated the correlation of $L_{\rm IR}$ with either $L_{{\rm Br}\alpha}$ or $L_{\rm PAH3.3}$ in ULIRGs. They first found that $L_{{\rm Br}\alpha}$ correlates well with $L_{\rm PAH3.3}$, and hence they used $L_{\rm PAH3.3}$ to trace the star formation in faint targets for which the Brα lines were not detected. Then, they found that the ratio of $L_{{\rm Br}\alpha}$ to $L_{\rm IR}$ or $L_{\rm PAH3.3}$ to $L_{\rm IR}$ is much smaller for Seyfert

1/LINER-type ULIRGs than HII-type ULIRGs. From this result, they concluded that, in Seyfert 1/LINER ULIRGs, the contribution of starburst is 67% in the IR light, while the remaining 30% is from AGN.

4. DUST TORUS

In the AGN unification picture, the central engine of an AGN is surrounded by BLR clouds, and then by the dust torus which obscures the broad emission lines from the BLR clouds creating the observed dichotomy of type 1 and type 2 AGNs. The dust torus is commonly depicted to have an inner hot region that has the dust sublimation temperature of $T \sim 1500$ K (e.g., Barvainis 1987). The *AKARI* NIR spectral coverage of 2.5 to 5.0 μm allowed studies to test this picture in detail.

Using the QSONG low redshift AGN sample, Kim et al. (2015) combined the *AKARI* NIR spectra with the SDSS and *WISE* data and fitted the AGN SEDs using a three component model that is made of a power-law continuum component (mostly to fit the the optical data and the underlying flux in NIR), and two temperature black body component, one for the hot dust emission at a temperature of $T_{\rm HD}$ and another for the warm dust emission at a temperature of $T_{\rm WD}$. The model-fit results show that the hot dust component has the temperature of about 1100 K, a value significantly lower than the commonly cited hot dust torus temperature of 1500 K. Previously, Glikman et al. (2006) found a similarly low temperature (1260 K) for the hot dust component of type 1 AGNs. Landt et al. (2011) reported that a hot dust temperature of $\sim$ 1365 K. Our result is a bit lower than, but roughly consistent with these result indicating that the hot dust temperature is well below 1500 K. An independent study of the other *AKARI* data of AGNs by Oyabu et al. (2017) also shows that the hot dust temperature of around 1200 K. These results suggest that the sublimation temperature of the dust particles is colder than previously thought.

The *AKARI* NIR spectroscopy gives another unique way to investigate the dust torus. Baba et al. (2017) investigated AGN tori by observing CO ro-vibrational absorption band at 4.67 μm. The spectral data allowed them to investigate the $T_{\rm CO}$ and the column density $N_{\rm H}$, and they found that $T_{\rm CO} \sim$ 200–500 K and $\log(N_{\rm H} = 22\text{–}25\,{\rm cm}^{-2})$, a condition that can be explained with the heating by energetic photons from the AGN central engine. The column density is found to be high but not as high as the values estimated from X-ray data. Thus, Baba et al. (2017) concluded that CO band is tracing the inner ring of the obscuring materials around the AGN central engine.

5. STAR FORMATION FEEDBACK IN AGN

Star formation in galaxies can be either suppressed or enhanced due to AGN activities. To understand how the feedback works in AGNs, Karouzos et al. (2014) identified radio AGNs in the *AKARI* NEP survey field, and studied the interplay between SF activities and AGN activities. In this work, they found that the AGN activities correlate with the SF activities, suggesting a positive feedback in work. Here, the AGN activity is measured as from the SED fitting utilizing *AKARI*'s pan-chromatic IR imaging data and the ground-based ancillary imaging data (Jeon et al. 2014, 2010; Hwang et al. 2007). However, at a given redshift, they found that radio galaxies with stronger radio luminosities have weaker specific star formation rates (sSFRs). In this latter case, the radio luminosity represents the AGN jet activity. This implies that a negative feedback is present in radio AGNs, where jet activity suppresses SF activities. These two apparently contradictory feedback results in the radio AGNs indicate that the AGN feedback is two-sided, where both the suppression and triggering of star formation is possible.

The correlation of the FIR luminosity and the AGN luminosity was also investigated by Matsuoka & Woo (2015). In their work, they studied 492 type-2 AGNs with FIR detection in the *AKARI* and *Herschel* data. They found a correlation between the FIR and AGN luminosities, and a low fraction (1%) of the pure AGNs with low SF. However, their additional simulation analysis showed that the apparent low fraction of the pure AGNs with low SF could be due to the observational limitations, throwing a caution to this kind of correlation analysis with the current FIR survey data.

6. REST-FRAME OPTICAL SPECTRA OF HIGH REDSHIFT QUASARS

AKARI is the currently the only facility in the world that has succeeded in detecting the redshifted Hα lines of quasars at $z > 4$. The first detection of the redshifted Hα of a high redshift quasar was reported for RX J1759.4+6638 at $z = 4.3$ (Oyabu et al. 2007), where the IRC low resolution NIR prism clearly caught the Hα line at the observed wavelength of 3.47 μm. Note that this wavelength window is swamped with thermal emission noise when observing from the ground, so the detection of the high redshift Hα line is virtually impossible even with a deep spectroscopy using 10 m class telescopes.

The more extensive studies of the rest-frame spectra of high redshift quasars are presented in Im (2010, 2017) and Jun et al. (2015), together with the first detection of the redshifted Hα lines at $4.5 < z < 6$. This study was performed as a part of the *AKARI* mission program, QSONG, and a couple of PI-based open time programs, and used the *AKARI* IRC's prism and grism modes. These observing modes offered the slitless spectroscopy at $R = 20$ and 100 respectively, which were good enough for detecting the redshifted broad Balmer lines of AGNs at $4 < z < 6$. The grism mode even allowed one to measure the line widths with FWHM $\gtrsim$ 3000 km s^{-1}. Figure 5 shows the reference image and the slitless spectra of objects in the field surrounding a high redshift quasar, BR 0006-6208 at $z = 4.5$, to demonstrate how the observation was done.

Through QSONG, we obtained the rest-frame optical spectra of 155 high redshift quasars ($3.3 < z < 6.4$). Targets were selected based on apparent magnitude limits, $z \lesssim 19$ AB mag for $z < 5.5$ quasars, and $z \lesssim 20$ AB mag for $z > 5.5$ quasars.

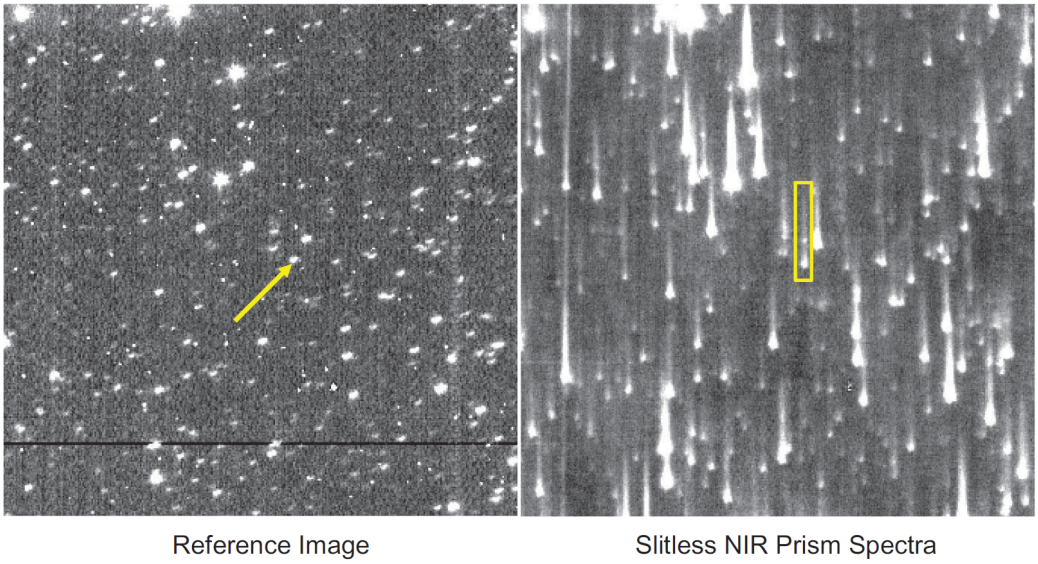

Figure 5. The reference image (left) and the slitless spectra (right) of the BR 0006-6208 field. Each tadpole-shaped vertical line in the slitless spectra image is the spectrum of each object. The spectrum of BR 0006-6208 at $z = 4.5$ is shown within a yellow rectangle near the middle of the image, showing a clear sign of an emission line over the continuum.

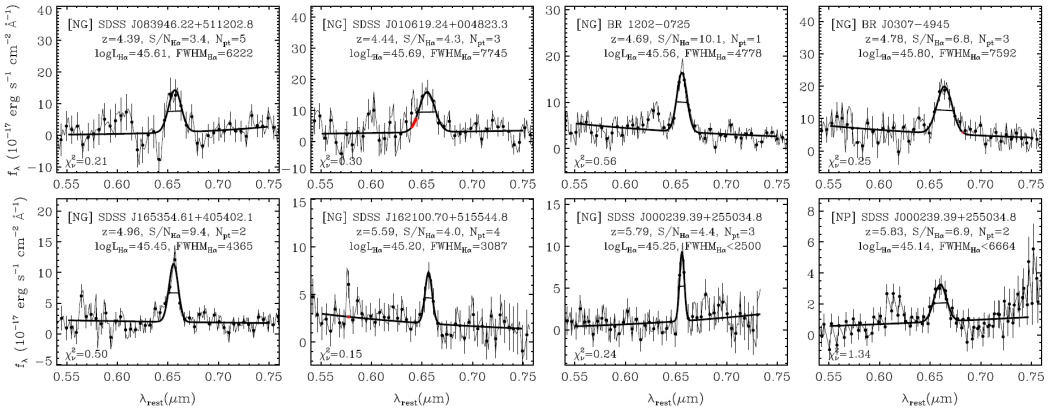

Figure 6. Examples of the *AKARI* spectra centered on Hα of high redshift quasars, demonstrating secure detection of the line and showing the best-fit model to measure the line luminosity and width values. Also indicated are the redshift and the object ID. The data with "*NG*" denote the grism data, while "*NP*" denotes the data taken in the prism mode.

This corresponds roughly to the bolometric luminosity and BH mass cuts at $L_{\rm bol} \sim 10^{47}$ erg s^{-1} and $M_{\rm BH} \sim 10^9\,M_\odot$ (Jun et al. 2015). The redshifted Hα lines were detected in 72 quasars with $S/N > 2$ at the peak wavelength element. Figure 6 shows examples of the *AKARI* spectra of the high redshift Hα lines.

Using the *AKARI* spectra, Jun et al. (2015) obtained the Hα luminosity ($L_{\rm H\alpha}$) and the 5100 Å continuum luminosity (L_{5100}) and found that the high redshift quasars follow the same scaling relation as the lower redshift counterparts. This result has several interesting implications. First, the photo-ionization models of BLRs suggest that the continuum luminosity from the accretion disk should be proportional to the emission line luminosity. Figure 7 confirms that this is true for a wide range of L_{5100} over six orders of magnitude in luminosity. Second, this scaling relation is universal from low to high redshift. The addition of the *AKARI* data points extends the validity of the luminosity scaling relation to $z \sim 6$. The AGN physics seems to be identical at $z = 0$ and $z = 6$, giving a justification to use various AGN scaling relations such as $M_{\rm BH}$ estimators at low redshift for studying high redshift AGNs. Third, the linear relation between $L_{\rm H\alpha}$ and L_{5100} suggests high spin of SMBHs at high redshift. Several models expect that spin can be low (the specific angular momentum $a < 0$) for massive BHs (Laor & Davis 2011; Wang et al. 2014), which decreases the ionization flux in UV from the accretion disk whose temperature became low due to the low spin. Consequently, these models expect that the $L_{\rm H\alpha}$–L_{5100} relation to break down at high luminosity end. This, however, is not observed in Figure 7, meaning that a should be well above 0 (Jun et al. 2015).

Jun et al. (2015) also estimated $M_{\rm BH}$ of high redshift quasars from Hα (denoted as $M_{\rm BH,H\alpha}$), and compared them against the CIV-based $M_{\rm BH}$ values, $M_{\rm BH,CIV}$. Figure 8 shows this comparison for both $3.3 < z < 6.0$ quasars in the *AKARI* QSONG sample and the lower redshift sample ($0 < z < 3.8$) from literature. The comparison shows that the $M_{\rm BH,CIV}$ values agree with the $M_{\rm BH,H\alpha}$ values on average, but with a rather large rms scatter of 0.4 dex. A smaller rms scatter of 0.1-0.2 dex is observed for Mg II-based $M_{\rm BH}$ values against $M_{\rm BH,H\alpha}$ values, although for the Mg II-based $M_{\rm BH}$ values, only quasars at $z < 3.8$ are used. The *AKARI* measurements from the rest-frame optical spectra of high redshift quasars place the previously reported discoveries of billion solar mass BHs on a more secure footing.

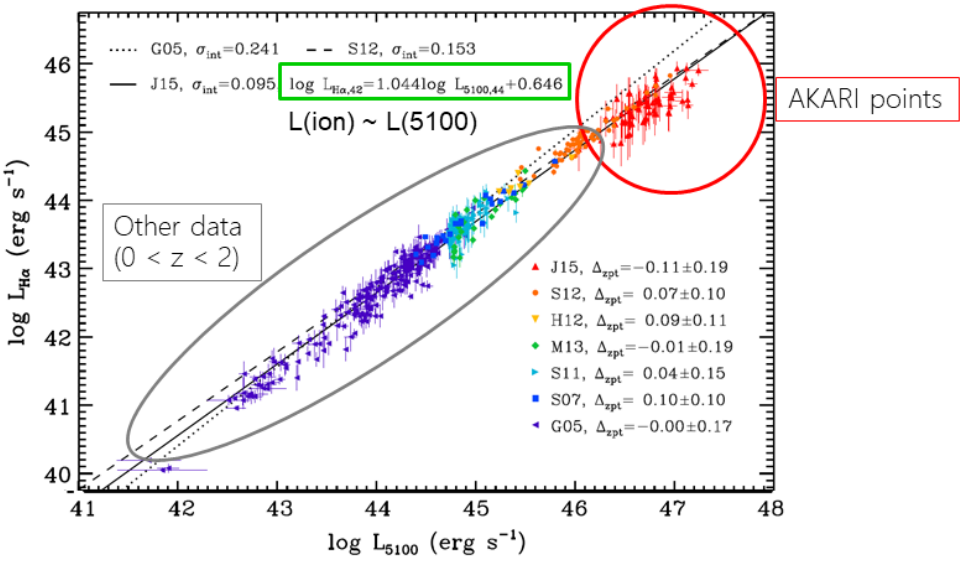

Figure 7. Comparison of the Hα luminosity ($L_{\rm H\alpha}$) versus the 5100 Å luminosity (L_{5100}) of AGNs. The *AKARI* points (red dots) provide the high luminosity data for AGNs at $3.3 < z < 6$. This figure shows that, from $z = 0$ to $z = 6$, the luminosity scaling relation is well described by a linear relation, consistent with a photo-ionization model of BLRs and fast-spinning BHs in the early universe. The validity of the scaling relation provides a justification for using the low redshift $M_{\rm BH}$ estimators to high redshift AGNs. A modified version of Figure 11 in Jun et al. (2015).

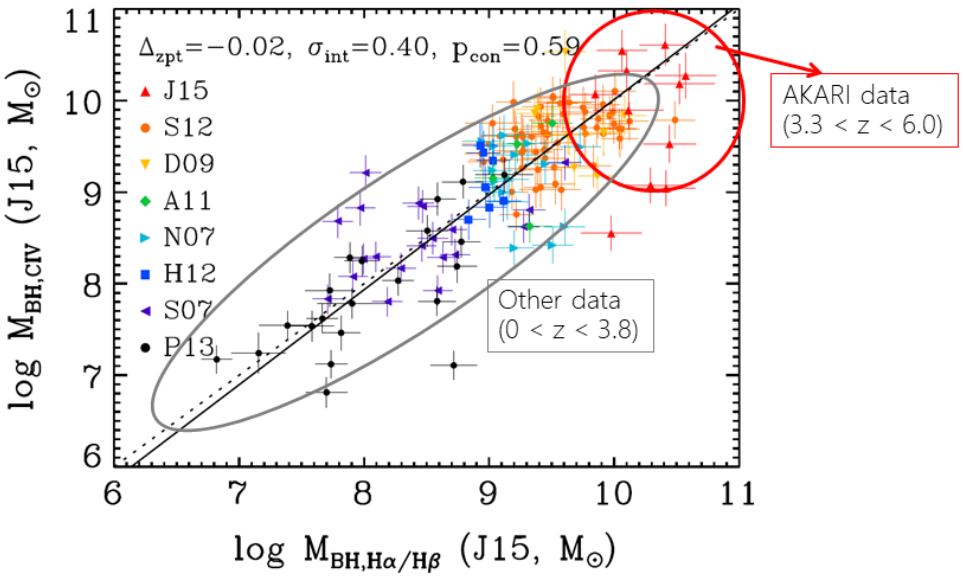

Figure 8. Comparison of the $M_{\rm BH}$ estimates from the CIV line versus those from the Hα line from *AKARI* observation. *AKARI* provides data points at $3.3 < z < 6.0$, revealing that the $M_{\rm BH,CIV}$ values agrees with $M_{\rm BH,H\alpha}$ on average but with a large dispersion (0.4 dex in rms). Despite of the large scatter, this result suggests that the CIV-based $M_{\rm BH}$ estimates can be trusted within the derived scatter. The result also validates the very large BH masses of high redshift quasars ($M_{\rm BH} \gtrsim 10^9\,M_\odot$) that are measured from the UV metal lines. Taken and modified from Figure 15 in Jun et al. (2015).

7. SUMMARY

AKARI has produced many pioneering results about AGNs, ranging from the MIR selection of AGNs, to the rest-frame optical spectra of high redshift quasars out to $z = 6$. Although small in the primary mirror aperture size (0.67 m), the cold and the atmosphere-free environment of the space allowed *AKARI* make this remarkable achievement. Future facilities such as JWST are much more powerful than *AKARI*, and the current results from *AKARI*, already great, make us foresee what kind of far greater discoveries to be made in future.

ACKNOWLEDGMENTS

This research is based on observations with *AKARI*, a JAXA project with the participation of ESA. This work was supported by the National Research Foundation of Korea (NRF) grant, No. 2017R1A3A3001362, funded by the Korea government. We thank colleagues who participated in QSONG, especially Hyung Mok Lee, Hyunsung Jun, Dohyeong Kim, Youichi Ohyama, and Takao Nakagawa for their key contributions to the program. We also thank other colleagues who provided their interesting results for this review presentation.

REFERENCES

Baba, S., Nakagawa, T., Isobe, N., & Shirahata, M. 2017, ApJ, in press
Barvainis, R. 1987, ApJ, 320, 537
Glikman, E., Helfand, D. J., & White, R. L. 2006, ApJ, 640, 579
Hanami, H., Ishigaki, T., Fjushiro, N., et al. 2012, PASJ, 64, 70
Hwang, H. S., & Geller, M. J. 2013, ApJ, 769, 116
Hwang, N., Lee, M. G., Lee, H. M., et al. 2007, ApJS, 172, 583
Im, M. 2017, PKAS, 32, 163
Im, M. 2010, in IAU Symp. 267, Co-Evolution of Central Black Holes and Galaxies, ed. B. M. Peterson, R. S. Somerville, & T. Storchi-Bersmann (Cambridge: Cambridge Univ. Press), 40
Imanishi, M., Maiolino, R., & Nakagawa, T. 2010a, ApJ, 709, 801
Imanishi, M., Nakagawa, T., Shirahata, M., Ohyama, Y., & Onaka, T. 2010b, ApJ, 721, 1233
Isobe, N., Kwamuro, T., Oyabu, S., et al. 2016, PASJ, 68, 98
Jarrett, T. H., Cohen, M., Masci, F., et al. 2011, ApJ, 735, 112
Jeon, Y., Im, M., Kang, E., Lee, H. M., & Matsuhara, H. 2014, ApJS, 214, 20
Jeon, Y., Im, M., Ibrahimov, M., Lee, H. M., Lee, I., & Lee, M. G. 2010, ApJS, 190, 166
Jun, H., Im, M., Lee, H. M., et al. 2015, 806, 109
Karouzos, M., Im, M., Trichas, M., et al. 2014, ApJ, 784, 137
Kawada, M., Baba, H., Barthel, P. D., et al. 2007, PASJ, 59, 389
Kim, D., Im, M., Kim, J. H., et al. 2015, ApJS, 216, 17
Kim, D., Im, M., & Kim, M. 2010, ApJ, 724, 386
Kim, J. H., Im, M., Lee, H. M., et al. 2012, ApJ, 760, 120
Krumpe, M., Miyaji, T., Brunner, H., et al. 2015, 446, 911
Landt, H., Elvis, M., Ward, J., et al. 2011, MNRAS, 414, 218
Laor, A., & Davis, S. W. 2011, MNRAS, 417, 681
Lee, H. M., Kim, S. J., Im, M., et al. 2009, PASJ, 61, 375
Lee, H. M., Im, M., Wada, T., et al. 2007, PASJ, 59, 529
Lyu, J., & Rieke, G. H. 2017, ApJ, 841, 76
Mateos, S., Alonso-Herrero, A., Carrera, F. J., et al. 2012, MNRAS, 426, 3271
Matsuhara, H., Wada, T., Matsuura, S., et al. 2006, PASJ, 58, 673
Matsuoka, K., & Woo, J- H. 2015, ApJ, 807, 28
Murakami, H., Baba, H., Barthel, P., et al. 2007, PASJ, 59, 369
Onaka, T., Matsuhara, H., Wada, T., et al. 2007, PASJ, 59, 401
Oyabu, S., Kaneda, H., Izuhara, M., et al. 2017, PKAS, 32, 157
Oyabu, S., Wada, T., Ohyama, Y., et al. 2007, PASJ, 59, 497
Shim, H., Im, M., Ko, J., et al. 2013, ApJS, 207, 37
Urrutia, T., Becker, R. H., White, R. L., et al. 2009, ApJ, 698, 1095
Urry, C. M., & Padovani, P. 1995, PASP, 107, 803
Vestergaard, M., & Peterson, B. M. 2006, ApJ, 641, 689
Wang, J.-M., Du, P., Li, Y.-R., Ho, L. C., Chen, H., & Bai, J.-M. 2014, ApJ, 792, L13
Yamada, R., Oyabu, S., Kaneda, H., et al. 2013, PASJ, 65, 103
Yano, K., Nakagawa, T., Isobe, N., & Shirahata, M. 2016, ApJ, 833, 272